EXPERIMENTAL TECHNIQUE AND DEVICES

Original article
DOI: https://doi.org/10.18721/JPM.16409

AN EXPERIMENTAL APPARATUS FOR STUDYING THE CHARACTERISTICS OF THERMOELECTRIC EFFECT IN NANOSTRUCTURES

K. R. Trofimovich, P. G. Gabdullin, A. V. Arkhipov✉

Peter the Great St. Petersburg Polytechnic University, St. Petersburg, Russia

✉ arkhipov@rphf.spbstu.ru

Abstract. We present an experimental setup for the study of thermoelectric effect in point contacts between different materials and in nanostructures. Point contacts of controlled size are formed with the use of an atomic force microscope (AFM), thermopower dependences against the temperature drop and against the contact spot size determined from the force applied to the probe. Computer simulations of heat transport in the system were performed to evaluate influence of atmospheric air and of a liquid layer covering solid surfaces in the atmospheric conditions onto temperature distributions. This influence was found to be insubstantial, which makes it possible to conduct experiments on the atmosphere and not in high vacuum.

Keywords: thermoelectric effect, point contact, nanostructures, atomic force microscope

Funding: The reported study was funded by Russian Science Foundation (Grant No. 23-29-10027 (https://rscf.ru/project/23-29-10027/) and by St. Petersburg Science Foundation (Grant No. 23-29-10027).

Citation: Trofimovich K. R., Gabdullin P. G., Arkhipov A. V., An experimental apparatus for studying the characteristics of thermoelectric effect in nanostructures, St. Petersburg State Polytechnical University Journal. Physics and Mathematics. 16 (4) (2023) 101–117. DOI: https://doi.org/10.18721/JPM.16409

Научная статья
УДК 538.93, 536.241
DOI: https://doi.org/10.18721/JPM.16409

ЭКСПЕРИМЕНТАЛЬНАЯ УСТАНОВКА ДЛЯ ИССЛЕДОВАНИЯ ОСОБЕННОСТЕЙ ТЕРМОЭЛЕКТРИЧЕСКОГО ЭФФЕКТА В НАНОСТРУКТУРАХ

К. Р. Трофимович, П. Г. Габдуллин, А. В. Архипов✉

Санкт-Петербургский политехнический университет Петра Великого,

Санкт-Петербург, Россия

✉ arkhipov@rphf.spbstu.ru

Аннотация. Представлены общая схема и конструкция экспериментальной установки для изучения термоэлектрических явлений в точечных контактах разнородных материалов и в наноструктурах. Точеные контакты регулируемого размера формируются с помощью атомно-силового микроскопа, определяются зависимости термоэдс от разности температур и от силы воздействия зонда на образец. Проведено численное моделирование распределения температуры в такой системе для различных условий, оценено влияние воздушной среды и жидкого слоя, формирующегося на поверхностях в условиях естественной атмосферы. Моделирование показало, что это влияние не является существенным, что делает необязательным проведение экспериментов в высоком вакууме.

Ключевые слова: термоэлектрический эффект, точечный контакт, наноструктуры, нанотеплофизика, атомно-силовой микроскоп

Финансирование: Исследование выполнено за счет гранта Российского научного фонда № 10027-29-23 (https://rscf.ru/project/23-29-10027/) и гранта Санкт-Петербургского научного фонда № 23-29-10027.

Ссылка для цитирования: Трофимович К. Р., Габдуллин П. Г., Архипов А. В. Экспериментальная установка для исследования особенностей термоэлектрического эффекта в наноструктурах // Научно-технические ведомости СПбГПУ. Физико-математические науки. 2023. Т. 4 № .16. С. 101–117. DOI: https://doi.org/10.18721/JPM.16409

Introduction

The problem of increasing energy efficiency is becoming more and more urgent for electronics. It was reported, in particular, that more than 10% of the world's electricity is already consumed by computers and telecommunications equipment, and this share is growing rapidly [1]. The energy consumed by electronic devices is eventually released as heat, and the reverse conversion of some of this heat into electricity could significantly increase overall energy efficiency. The most natural way to utilize the thermal energy of electronic components is the use of solid-state thermoelectric generators (TEG). The development and improvement of TEG has been underway for many years (at least since the 1940s), and substantial advances have been made. However, there are fundamental physical limitations to increasing the effectiveness of TEG.

Thermoelectric materials are commonly evaluated by the parameter of thermoelectric performance (quality) Z or, more often, the dimensionless quantity of the same name ZT, where T is the absolute temperature. This parameter characterizes the difference between the efficiency of thermoelectric conversion, achievable using the material, and the efficiency of an ideal heat engine. The dependence of the thermoelectric performance on the properties of the material is given by the formula [1–4]:

$$ZT = \frac{S^2 \sigma T}{\kappa_{el} + \kappa_{ph}}, \quad (1)$$

where S is the Seebeck coefficient (defined as the coefficient of proportionality between the thermopower and the temperature drop); σ is electrical conductivity; κ_{el}, κ_{ph} are the electron and lattice (phonon) components of thermal conductivity.

According to available estimates, the widespread use of TEG in the energy sector will be economically justified when ZT = 3–4 is reached. The ZT values obtained so far for the best thermoelectric materials (in particular, bismuth telluride Bi_2Te_3) at room temperature are close to unity. It is obvious from Eq. (1) that to increase the thermoelectric performance, it is necessary to reduce the thermal conductivity of the material and increase its electrical conductivity and the Seebeck coefficient. Metals, due to their high electrical conductivity, are not optimal materials for TEG, since the values of the Seebeck coefficient are small: in most cases they do not exceed10 MV/K in absolute value. In addition, the heat flow in metals is carried mainly by electric charge carriers, so consequently the thermal and electrical conductivity of metals in the denominator and numerator of Eq. (1), respectively, are proportional to each other (Wiedemann–Franz law), which makes it difficult to optimize the ZT parameter. In contrast, semiconductors have low electronic thermal conductivity, and the heat flow in them is carried almost exclusively by phonons. The Seebeck coefficient of semiconducting materials is usually quite large (hundreds of μV/K), which is determined by significant variations in the energy density function of electron states near the Fermi level [3–5]. The thermoelectric properties of semiconductors can be optimized by choosing the degree of their doping [6, 7] or by shifting the Fermi level in other ways [8]. In general, semiconductors are characterized by the best thermoelectric parameters among homogeneous bulk materials, but the possibilities for their radical improvement are still limited.

In recent decades, the prospects for the creation of commercially successful thermoelectric devices have been associated with nanostructures and nanostructured materials. Many experiments (see, for example, [9–12]) have fundamentally confirmed the theoretical predictions made by in [4, 13] about the possibility of using size effects to selectively reduce thermal conductivity due to the scattering of phonons by interfaces and defects, with less influence on electrical conductivity.

It is equally promising to construct thermoelectric devices using nanoparticles, individual molecules or molecular layers [2, 3, 12–16] with a discrete spectrum of allowed electronic states, which can be optimized to achieve high values of S and ZT. Nanostructures developed can provide conditions simultaneously for destructive interference of lattice excitations and constructive interference of electronic waves [1, 2]. Calculating the thermoelectric parameters of devices using nanoscale elements is a difficult problem, which increases the role of experiment in such studies.

Problem statement

This paper presents the results of the first, initial stage of a new research project, whose purpose is to experimentally verify one of the theoretical models predicting the possibility of constructing a high-efficiency TEG based on heat transfer characteristics and thermoelectric phenomena in carbon-based nanostructures.

Carbon in the state of sp^2-hybridization (single-layer and multilayer graphene, carbon nanotubes, graphite) has unique characteristics [4, 17, 18]: low effective mass of charge carriers, high thermal conductivity, high light absorption coefficient. The electronic properties of graphene and carbon nanotubes are easily modified not only by doping and defects, but also by an electric field, which makes carbon in the state of sp^2-hybridization a promising material for electronics. Among other things, the possibility of its use as part of thermoelectric devices was also considered [5, 19].

Eidelman proposed [20, 21] a TEG based on a structure of nanometer layers of diamond-like and graphite-like carbon. The principle of its operation is based on the theoretical model proposed in Eidelman's earlier studies [22, 23], which substantiates the possibility of obtaining increased values of the Seebeck coefficient S and the ZT parameter using the phenomenon of charge-carrier entrainment by ballistic flow of phonons, even at room and higher temperatures. In this case, to achieve a positive result, localization of the electric field and temperature drop in a planar sp^2-carbon nanolayer is required, where the phonon flow remains ballistic. The diamond-like layer plays the role of a cooler, diverting the unused part of this flow. The presence

of sharp (no more than several lattice spacings) interphase boundaries is also seen as a necessary condition. In our opinion, the experimental demonstration of the predicted effect in [21] was not entirely convincing. The reason for this was probably the objective technological complexity of forming the ideal structure required by the theory; the presence of defects, almost inevitable at the specified values of thickness and area, could lead to electrical shorting of the real structure and a decrease in the thermoelectric voltage recorded for it.

Our study is aimed at conducting an experimental verification of the viability of the concept proposed in [20, 21] using a structure that is easier to create, whose main part is, for example, a carbon nanostructure on the surface of a silicon substrate (serving in this case as a cooler or, conversely, a heater). The second thermal and electric contact with the island should be established by means of an atomic force microscope (AFM) probe. We have previously studied island-type carbon films of the required structure in connection with their ability to emit electrons [24–26].

The advantage of the proposed approach is the possibility of conducting quick independent testing of the thermoelectric properties of many islands, which differ in size and properties of the interface with the substrate. This seems necessary because we expect that only a few of the islands will show high thermoelectric performance.

Such expectations are associated with important features introduced by thermal contacts of small lateral dimensions.

The phenomenon of a decrease in thermopower in nanocontacts is known [27–30], which is explained precisely by the suppression of phonon entrainment of charge carriers. Its cause is seen in the scattering of nonequilibrium phonons at the aperture of the nanocontact, which reduces the likelihood of transmitting their momentum to electrons or holes. Therefore, according to the theory outlined in [27], an additional multiplier $d/Л_p$ appears in the formula for thermal entrainment for small contact diameters d, where $Л_p$ is the phonon path length.

The experiments planned are intended for studying islands whose height is of the order of the phonon path length, approximately equal to 5 nm (according to the estimate in [21]). Their lateral size will be several times larger, but the size of the contact with the AFM probe may be small and poorly controlled.

However, according to many researchers, the boundary scattering of phonons is only one of the reasons for the dependence of the Seebeck coefficient and other kinetic coefficients on the size of the contact region. In particular, both theoretic predictions and experimental observations exist for deviation of the kinetic dependences from the linear form upon violation of the condition $L_T > \Lambda_p$, where L_T is the distance at which the temperature changes significantly; it can be defined, for example, as

$$L_T^{-1} = \max\left(\frac{|\text{grad } T|}{T}\right). \tag{2}$$

The reason for this phenomenon is seen in the nonlocality of the interaction of charge carriers with the lattice [31–37]. If the condition $L_T > \Lambda_p$ is violated, it cannot be assumed that the interaction occurs at a point with certain coordinates. Often, the temperature value also cannot be correctly determined, since the distributions of phonons and charge carriers turn out to be significantly nonequilibrium [5, 38]. One of the manifestations of non-locality is the dependence of the thermopower value not only on the applied temperature difference, but also on its distribution profile, on the maximum value of its gradient, i.e., on the characteristics that can hardly be predicted for the thermal contact of the probe with the island.

Another region with properties that vary greatly from island to island may be the interface with the substrate, since the islands were formed on a layer of natural oxide; notably, it is stated in the literature [30, 39, 40] that thin intermediate layers do not affect the results of measuring the thermoelectric parameters of coatings and nanostructures.

For these reasons, reliable detection of high values of the Seebeck coefficient (the estimate of its expected value in [21] is 50 mV/K) for at least a small part of carbon nanostructures (or other similar samples) brought into contact with the AFM probe with an excellent temperature can be considered as confirmation of theoretical predictions of [20–23] and will become an incentive for subsequent efforts on the practical implementation of the concept of TEG proposed in [21].

Experimental setup

An experimental setup for solving the above problem is currently developed based on NanoDST AFM (Pacific Nanotechnology, USA). This approach should not be considered new: setups based on probe microscopes have been successfully used in similar studies, in particular, to map the distributions of thermal and thermoelectric parameters [5, 6, 39–44] and to study the properties of molecular layers and individual molecules [1, 5, 16, 39, 45]. The novel characteristics of the setup developed are minimal improvements to the serial AFM and the use of standard AFM probes in its operation, which is possible since a limited range of problems will be solved at the initial stage of research.

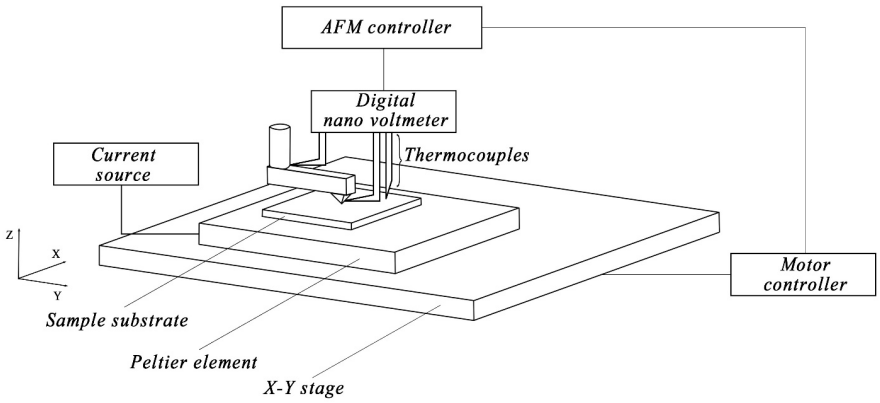

Fig. 1. Schematic of experimental setup

The experimental setup is shown schematically in Fig. 1. The large positioning stage (X-Y stage) and the probe holder play the role of thermostats with the temperature equal to the ambient temperature T_0. The sample substrate considered is placed on the upper surface of the Peltier element, whose temperature is maintained (using the Current source feeding the element) at a set value $T = T_0 + \Delta T$. The temperature values are controlled by thermocouples. During the experiment, the AFM probe, whose initial temperature is T_0, is brought into contact with the point of the sample selected during a preliminary scan of its surface. The thermoelectric voltage formed during contact is recorded by a digital nanovoltmeter synchronized with the AFM controller. Simultaneous recording of its reading and the force-distance curve of the AFM allow to determine the dependence of the thermoelectric voltage on the force of interaction of the probe with the surface, and therefore on the size d of their contact region. To isolate the voltage component associated with the contact potential difference, the experiment is also carried out for $\Delta T = 0$.

The problem of determining purely thermal parameters, i.e., the values of heat flows, thermal resistance, thermal conductance and thermal conductivity, is usually the most difficult from the standpoint of measurement technology [38, 46, 47]. At this stage, we neglected to define them, since to assess the applicability of the TEG concept proposed in [21], it is sufficient to find the maximum values of the Seebeck coefficient S, i.e., temperature and thermopower measurements. If reproducible dependencies $S(\Delta T)$ and $S(d)$ are found, the results obtained will provide additional information about the physics of heat and electric charge transfer processes in the system considered.

In the future, it is planned to expand the capabilities of the setup.

Experimental samples

The following samples were selected for the first experiments (below they are given in sequence from simple to more complex).

Nanocontact of AFM probe with a metal plate or thick (Cu, Au) film. Since the values of the Seebeck coefficient for silicon significantly exceed its values for metals, when a silicon probe comes into contact with a metal plate, it is natural to expect that the value of the thermopower will be mainly determined by the processes in the probe. Thus, the main purpose of such experiments is to determine the contribution of probes of different types to thermopower: with a metal

coating and without a coating, with a different size of the contact spot. Such data are necessary for conducting subsequent experiments with other objects, that is, to take into account the contribution of the AFM probe to the recorded values of thermopower.

Nanocontact of AFM probe with silicon plate. Measurements of the thermoelectric characteristics of nanocontacts formed between AFM probes and substrates are very important for the correct interpretation of other experimental results, since carbon nanostructures (these are the main objects of experiments at this stage of the study) are formed on silicon substrates. However, there is an additional motivation for conducting such experiments.

Island films of carbon and metals (molybdenum, zirconium, tungsten) formed on silicon substrates were found to be capable of low-voltage field emission in previous experiments [24, 25, 48]. It was suggested that thermoelectric potentials play an important role in the physical mechanism of the emission process [26, 48, 49]. At the same time, the absence of significant differences in the emission parameters of carbon and metal islands indicated that thermoelectric potentials are formed not in the islands themselves, but in substrates near the islands. A theoretical consideration of such a process using a model of charge carrier entrainment by ballistic phonon flow [21] made it possible to evaluate the effectiveness of thermoelectric conversion by such a structure. The results of this analysis will be published later, and they may be important in connection with the objectives of this study. This is reason for additional interest in the results of the planned experimental testing of thermoelectric characteristics of nanocontacts of metallized probes with silicon substrates.

Admittedly, the properties of silicon point contacts have already been studied before, from the 1980s to the 1990s. However, these early experiments were carried out mainly with contacts of micron and submicron sizes (20–0.3 μm) [29, 30, 50], which were formed between the pointed edges of silicon wedges pressed against each other with a force of 1–100 mN [50]. Mechanical compression led to the appearance of significant deformations in the near-contact region, which, according to the authors [30], were capable of causing additional scattering of phonons and influencing the propagation of heat flows. The size of the contact between the AFM probe and the planar surface and the force of their interaction can be significantly reduced to more correctly simulate the contact of the substrate with the nanostructure formed on it. The nominal value of the elastic constant of the CSG01 AFM probe (NT MDT, Russia), designed for contact mode measurements, is 0.03 N/m. The transition from attractive forces to repulsive forces on a typical force-distance curve of an AFM probe (when direct contact of the probe with the surface is established) occurs at a distance of about 100 nm [41, 42]. These values can be used to estimate the strength of the mechanical interaction of the probe with the sample surface as $F \approx 3 \cdot 10^{10}$ N. The diameter of the contact spot d can be calculated by solving the problem of the elastic interaction of a sphere of radius R and a plane [41]:

$$d = \left(\frac{6FR}{E} \right)^{1/3}, \tag{3}$$

where E is Young's modulus (E = 109 GPa for silicon), R is the probe tip radius.

For the nominal value R = 10 nm, this gives an estimate of the minimum diameter of the contact spot $d \approx 1.2$ nm. When the pressure reaches the plastic limit (for example, in the case of a metal plate), this value may increase slightly, but it certainly will not exceed the radius of the tip [41]. Thus, the size of the contact spot between the AFM probe and the silicon or metal plate can be made significantly smaller than the corresponding values achieved in classical studies [29, 30, 50]. Comparing their results may be of considerable interest.

Carbon nanostructures and graphene sheets (sp^2-carbon). As already mentioned above, the thermoelectric properties of carbon nanostructures are considered as the main object of this study. Another object are sheets of multilayer graphene with a large interface area with the substrate and representing a closer equivalent of the proposed TEG prototype structure. The use of AFM makes it possible to establish thermal and electrical contact with the local area of a separate sheet of multilayer graphene and vary the force with which it is pressed against the surface of the substrate.

Images and surface profiles of samples of naturally oxidized silicon plates with carbon nanowires and graphene sheets of different areas are shown in Fig. 2, *a*–*c*. They were obtained using NanoDST AFM (Pacific Nanotechnology), which is planned to be used in thermoelectric experiments.

Metal nanoparticles. A feature of nanoscale particles in comparison with bulk materials is the discrete nature of the spectrum of resolved states. This feature is favorable in terms of the possibility of achieving high thermoelectric performance. In accordance with the well-known Mott formula, the Seebeck coefficient is determined by the value of the derivative of the energy density of states at the Fermi level [4]:

$$S = \frac{\pi^2 k_B^2 T}{3e} \left\{ \frac{d\left[\ln\left(\sigma(\varepsilon)\right)\right]}{d\varepsilon} \right\}_{\varepsilon=\varepsilon_F}, \qquad (4)$$

where k_B is the Boltzmann constant, ε_F is the Fermi energy, $\sigma(\varepsilon)$ is the value of the differential contribution of charge carriers with energy ε to electrical conductivity.

It should be borne in mind that Eq. (4), generally speaking, refers to metals and degenerate semiconductors and may not be completely correct for sp^2-carbon. However, it is useful for understanding general trends: in the vicinity of a discrete energy level, all energy derivatives are large, which, at the optimal position of the Fermi level, can provide a large value of the Seebeck coefficient [3]. Varying the parameters, namely, particle size, electric potential, etc., allows to "adjust" the relative position of the Fermi level and the permitted energy levels, optimizing it to achieve high thermoelectric performance.

A comparison of the thermoelectric properties of carbon and metal nanoparticles can make it possible to separate the influence of size effects from the influence of the electronic structure of specific materials. 2,*d* shows the AFM image and the surface profile of tungsten nanoparticles for a sample formed on a silicon substrate and prepared for study; the substrate is identical to those used in other cases.

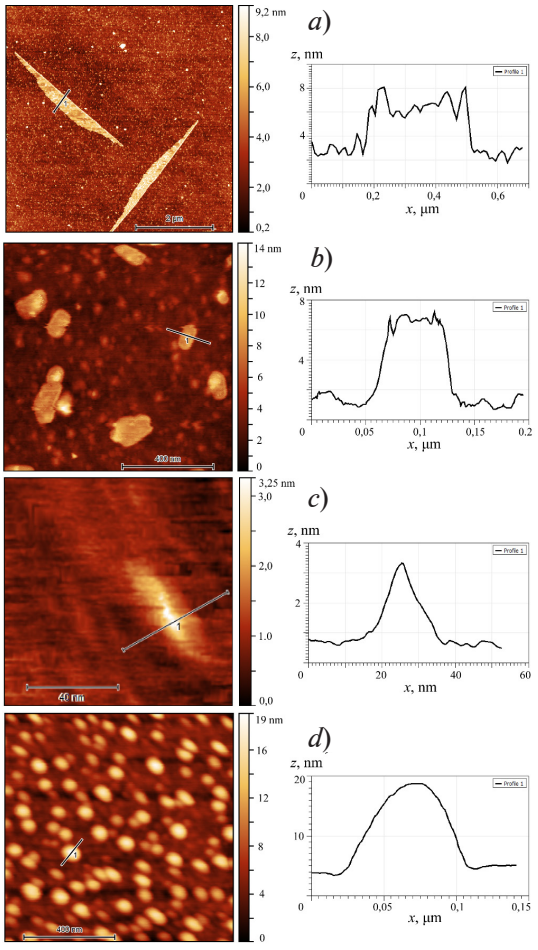

Fig. 2. AFM images (left) and surface topography profiles of nano-objects (right) on naturally oxidized silicon substrates. Nano-objects: sheets of multilayer graphene of large (*a*) and small (*b*) sizes, small carbon nanostructures (*c*) and metal nanoparticles of tungsten (*d*)

Numerical simulation

Numerical simulation of the temperature distribution over the contact region of the AFM probe with a planar substrate was carried out during the general planning of the experiment. The COMSOL Multiphysics software package implementing the finite element method was used. The package generally allows searching for numerical solutions to systems of differential equations of almost any kind with a given geometry and a set of boundary/initial conditions; this includes systems that take into account size effects and nonlocality; for example, equations from theoretical studies [32–37]. However, only the temperature distribution (but not the thermoelectric potential) was modeled at this stage of the research, and standard equations of the macroscopic theory of heat transfer and tabular values of thermal parameters of materials were used. This approach used because the modeling problems at this stage (experiment planning) were limited.

Let us present the basic requirements for these problems.

First, it was necessary to determine whether local temperature measurements near the

nanocontact region were necessary or whether it was sufficient to determine the temperatures of the sample substrate and the massive part of the AFM probe holder. To do this, it was actually necessary to estimate how much of the total temperature drop between these parts (whose temperature is easy to measure) falls on the cantilever of a standard probe under typical experimental conditions.

Secondly, it was necessary to determine whether measurements in vacuum conditions were required or an experiment in atmospheric conditions was acceptable. For this purpose, we had to assess the degree of influence of the ambient air and the equilibrium adsorbate layer on free surfaces on the temperature distribution in the nanocontact region.

Thirdly, it was necessary to determine whether it was possible to use a standard metallized probe as a metal electrode of a metal/sp^2 carbon or metal/semiconductor nanocontact.

Fourthly, it was necessary to estimate the time to establish the temperature distribution after the formation of the nanocontact under the conditions of the planned experiments.

To solve these problems, we estimated the temperature drops primarily on the auxiliary elements of the experimental device (primarily on the AFM probe cantilever), whose characteristic dimensions are large enough for calculations according to standard theory to provide sufficient accuracy. Significant calculation errors could be expected for the nanocontact region itself (most likely, towards lower thermal conductivity), which was taken into account in analysis of the results. We chose an experimental configuration with the requirement that most of the temperature drop created was concentrated in the nanocontact region. In this case, the maximum estimate of the expected value of the thermopower can be obtained by simply multiplying the temperature drop ΔT by the effective value of the thermoelectric coefficient S given by the theory (according to [21], it can reach 50 mV/K for the structure considered there).

Calculations of the temperature distribution were carried out by solving a standard equation of thermal conductivity of the form

$$\rho C_p \frac{\partial T}{\partial t} + \rho C_p \mathbf{u} \nabla T + \nabla \mathbf{q} = Q, \tag{5}$$

where ρ, C_p are the mass density and heat capacity of the substance; $\mathbf{u}$ is its local velocity (assumed to be identically equal to zero); $\mathbf{q}$ is the heat flow density; Q is the density of heat sources.

At this stage of the study, a linear relationship of the quantity $\mathbf{q}$ with the temperature gradient (Fourier's law) was postulated:

$$\mathbf{q} = -\kappa \nabla T, \tag{6}$$

where κ is the thermal conductivity.

The values of the material parameters given in Table 1 were used. The "Heat Transfer in Solids and Fluids" module of the COMSOL Multiphysics package was used, and the "Laminar Flow" module was also used to calculate heat transfer through the ambient air.

Table 1

Thermal parameters of materials used for simulation

Parameter	Parameter value for material			
	Si	Cu	Pt	Adsorbate (water)
Heat capacity, J/(kg·K)	700	375	133	4,200
Density, kg/m^3	2,329	8,960	21,450	1,000
Thermal conductivity, W/(m·K)	130	394	71.6	0.56

The contact of the AFM silicon probe with a copper substrate (thick plate) was simulated. The geometry of the tip and cantilever (Fig. 3,*a*, Table 2) was set in accordance with the parameters and image of the NSG10 probe provided on the manufacturer's website (NT-MDT, Russia). To simplify the calculations, a 2D problem was solved with the axis of symmetry passing through the center of the probe's contact region with a planar substrate. The shape of the tip of the probe was set as a cone conjugate to a sphere (Fig. 3,*b*). The radius of the sphere was taken to be 10 nm.

The same spherical surface was considered to be the interface of the tip with the substrate; it was assumed that the mechanical pressing action of the probe was strong enough for plastic deformation of copper in the contact region. The deviation of the 2D geometry from the true 3D geometry was compensated by setting the parameters of the cantilever material: its thermal conductivity and heat capacity in the left part (see Fig. 3,*a*) were set by tabular data, and then decreased along the radial coordinate according to the law $1/r$.

Table 2

Geometric parameters of AFM probe used in the simulation

Cantilever size, μm			Tip size, nm		Angle at cone vertex, degrees
Length	Width	Thickness	Height	Curvature radius	
125	27	3	$1.5 \cdot 10^4$	10	50

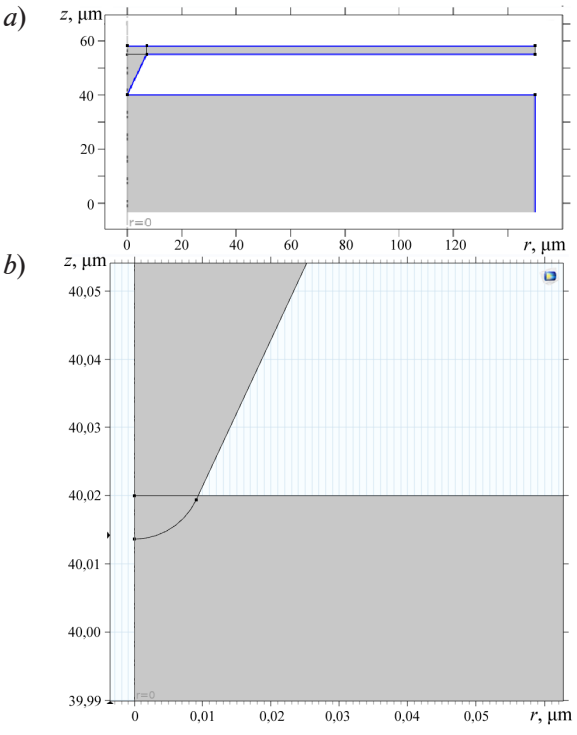

Fig. 3. Geometry of the problem of numerical simulation of temperature distribution over the nanocontact region of an AFM probe with a planar substrate: *a* is the general view, *b* is the nanocontact region

At the initial time, the substrate temperature was set to 0 °C, and the temperature of all parts of the probe was set to 100 °C (the specific values of these parameters do not affect the type of distribution if linear equations are used). Dirichlet boundary conditions were set for the lower boundary of the substrate (0 °C) and for the right end of the cantilever (100 °C). The problem of thermal conductivity was solved by simulating the steady-state temperature distribution, as well as the evolution dynamics of this steady state.

Fig. 4 shows the simulation results. The temperature distribution (see Fig. 4,*a*) was obtained for a silicon probe in contact with the clean surface of a copper plate in vacuum; heat transfer by electromagnetic radiation was considered insignificant [41]. As expected, under these conditions, the larger part of the temperature drop falls on the probe, whose material is characterized by lower thermal conductivity; the geometric factor (conical shape) also slightly increases its thermal resistance. The temperature changes significantly only in the probe region near the nanocontact, up to distances of the order of several magnitudes of its radius. The temperature drop on the cantilever is negligible: it obviously does not exceed 1% of the total temperature difference.

The simulation results for the steady-state temperature distribution in the presence of air are shown in Fig. 4,*b*. Heat flows through the air due to thermal conductivity and convection were taken into account. We can observe a continuous and approximately linear temperature variation in the gap between the plate and the cantilever. It is known from the literature [41, 51] that the total heat flow between the AFM probe and the substrate at atmospheric pressure is largely determined by convection. However, the calculation showed that the thermal conductivity of the cantilever is sufficient to prevent the convective heat flow from noticeably distorting the temperature distribution near the nanocontact and changing the temperature of the base (wide part) of the probe by more than a fraction of a percent of its total drop.

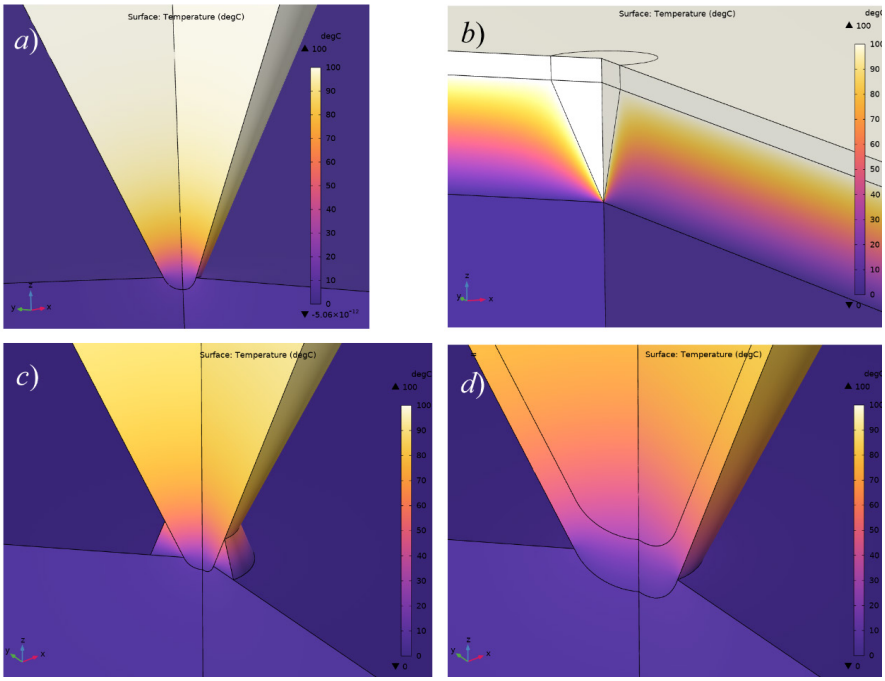

Fig. 4. Solution of the problem of thermal conductivity in the nanocontact region of AFM silicon probe with copper substrate.
Temperature distributions under vacuum conditions (*a*) are presented, taking into account thermal conductivity through air (*b*) and the presence of a liquid layer on the surface (*c*), as well as in the presence of a platinum metallization layer of the probe (*d*)

The above also applies to the influence of a layer of water and adsorbed gases covering free surfaces under normal conditions [41, 42]. To assess the degree of influence of the adsorbate on the temperature distribution, a circular layer (20 nm thick) with thermal conductivity of water was introduced into the model in the nanocontact region (see Fig. 4,*c*). Comparing the calculation result shown in Fig. 4,*c* with the data in Fig. 4,*a*, we can see that the influence of the liquid layer on the temperature distribution in the nanocontact is minimal.

Finally, the impact of metallization of the probe was assessed. The calculated results of the temperature distribution for a probe coated with a 30 nm thick platinum layer are shown in Fig. 4,*d*. Evidently, a significant part of the temperature drop falls precisely on the platinum layer, which has a relatively low thermal conductivity. Therefore, using platinum-coated probes in planned experiments is undesirable. It is preferable to use probes with a different coating, for example, made of gold (its thermal conductivity is 317 W/(m·K)) or another metal with high thermal conductivity (for example, copper or silver).

The simulation results for the dynamics of the steady-state temperature distribution evolving after the probe was brought into contact with the surface showed that in the absence of air, the characteristic time of such a process does not exceed several microseconds (Table 3). Such a delay can be neglected in experiments recording the AFM force-distance curve. As for the simulation of heat transfer through air, the stabilization time for the temperature distribution in the air to establish turned out to be significantly longer, amounting to milliseconds. However, this, apparently, should not interfere with measurements, since the heat flow through the air itself should have little effect on the temperature of the probe and the substrate, and temperature stabilization time for the contact area still amounts to microseconds. This conclusion is consistent with the literature data [45].

Thus, the numerical simulation carried out in a simplified COMSOL model allowed solving its main problem: to obtain a positive answer to the question of the possibility of conducting experiments to identify the features of the thermoelectric effect in atmospheric conditions using NanoDST AFM and standard probes.

Table 3

Simulated times for steady-state temperature distribution to establish under varying conditions

Condition	Stabilizatiion time, μs	
	Uncoated probe	Probe with platinum coating
Basic model (vacuum)	3.0	4.0
Atmospheric air	1.3	4.0
Liquid layer on surface	$4.0 \cdot 10^3$	$4.0 \cdot 10^3$
Air + liquid	$4.0 \cdot 10^3$	–

Conclusion

The paper presents the results of the initial stage of the research conducted at the Higher School of Engineering and Physics at Peter the Great St. Petersburg Polytechnic University and dedicated to the study of nanoscale features of the thermoelectric effect. The ultimate goal is to create thermoelectric generators with improved performance characteristics.

An experimental verification of the theory known from the literature describing the possibility of achieving high values of thermoelectric performance by using the phenomenon of entrainment of electric charge carriers by ballistic flow of phonons in a film nanostructure is chosen as the primary objective. We believe that the verification of this concept can be carried out by relatively simple means, namely, by measuring the thermoelectric characteristics of nanocarbon nanoislands and graphene sheets formed on a silicon substrate.

The results of numerical simulation indicate that such measurements can be carried out using an atmospheric atomic force microscope with standard probes after its retrofitting with systems for controlling and measuring the sample temperature.

REFERENCES

1. **Sadeghi H.,** Quantum and phonon interference-enhanced molecular-scale thermoelectricity, J. Phys. Chem. C. 123 (20) (2019) 12556–12562.

2. **Karlstrцm O., Linke H., Karlstrцm G., Wacker A.,** Increasing thermoelectric performance using coherent transport, Phys. Rev. B. 84 (11) (2011) 113415.

3. **Mahan G. D., Sofo J. O.,** The best thermoelectric, Proc. Natl. Acad. Sci. USA. 93 (15) (1996) 7436–7439.

4. **Dmitriyev A. S.,** Vvedeniye v nanoteplofiziku, 2-e izdaniye, elektronnoye [Introduction to nanothermophysics, Second electronic edition], "Laboratoriya Znaniy" Publishing, Moscow, 2020 (in Russian).

5. **Zevalkink A., Smiadak D. M., Blackburn J. L., et al.,** A practical field guide to thermoelectrics: Fundamentals, synthesis, and characterization, Appl. Phys. Rev. 5 (2) (2018) 021303.

6. **Lyeo H. K., Khajetoorians A. A., Shi L., et al.,** Profiling the thermoelectric power of semiconductor junctions with nanometer resolution, Science. 303 (5659) (2004) 816–818.

7. **Ikeda H., Salleh F.,** Influence of heavy doping on Seebeck coefficient in silicon-on-insulator, Appl. Phys. Lett. 96 (1) (2010) 012106.

8. **Salleh F., Suzuki Y., Miwa K., Ikeda H.,** Modulation of Seebeck coefficient for silicon-on-insulator layer induced by bias-injected carriers, Appl. Phys. Lett. 103 (6) (2013) 062107.

9. **Tretiakov O. A., Abanov Ar., Sinova J.,** Holey topological thermoelectrics, Appl. Phys. Lett. 99 (11) (2011) 113110.

10. **Krali E., Durrani Z. A. K.,** Seebeck coefficient in silicon nanowire arrays, Appl. Phys. Lett. 102 (14) (2013) 143102.

11. **Taniguchi T., Terada T., Komatsubara Y., et al.,** Phonon transport in the nano-system of Si and SiGe films with Ge nanodots and approach to ultralow thermal conductivity, Nanoscale. 13 (9) (2021) 4971–4977.

12. **Bergfield J. P., Solis M. A., Stafford C. A.,** Giant thermoelectric effect from transmission supernodes, ACS Nano. 4 (9) (2010) 5314–5320.

13. **Khvesyuk V. I., Scriabin A. S.,** Thermal conductivity of nanostructures, High Temperature. 55 (3) (2017) 428–450.

14. **Dubi Y., Di Ventra M.,** Colloquium: Heat flow and thermoelectricity in atomic and molecular junctions, Rev. Mod. Phys. 83 (1) (2011) 131–155.

15. **Sadeghi H., Sangtarash S., Lambert C. J**., Oligoyne molecular junctions for efficient room temperature thermoelectric power generation, Nano Lett. 15 (11) (2015) 7467–7472.

16. **Cui L., Miao R., Wang K., et al.,** Peltier cooling in molecular junctions, Nat. Nanotechnol. 13 (2) (2018) 122–127.

17. **Liu C., Lu P., Chen W., et al.,** Phonon transport in graphene based materials, Phys. Chem. Chem. Phys. 23 (46) (2021) 26030–26060.

18. **Varlamov A. A., Kavokin A. V., Luk'yanchuk I. A., Sharapov S. G.,** Anomalous thermoelectric and thermomagnetic properties of graphene, Phys.– Usp. 55 (11) (2012) 1146–1151.

19. **Wu Q., Sadeghi H., Garcна-Suбrez V. M., et al.,** Thermoelectricity in vertical graphene-C_{60}-graphene architectures, Sci. Rep. 7 (15 Sept) (2017) 11680.

20. **Eidelman E. D.,** On a carbon nanostructure-based thermoelectric converter with record parameters, Semicond. 51 (7) (2017) 906–908.

21. **Eidelman E. D.,** Thermoelectric effect and a thermoelectric generator based on carbon nanostructures: Achievements and prospects, Phys.–Usp. 64 (6) (2021) 535–557.

22. **Eydelman E. D., Vul' A. Ya.,** The strong thermoelectric effect in nanocarbon generated by ballistic phonon drag of electrons, J. Phys. Condens. Matter. 19 (7) (2007) 266210–266223.

23. **Koniakhin S.V., Eidelman E. D.,** Phonon drag thermopower in graphene in equipartition regime, Europhys. Lett. 103 (3) (2013) 37006.

24. **Andronov A., Budylina E., Shkitun P., et al.,** Characterization of thin carbon films capable of low-field electron emission, J. Vac. Sci. Technol. B. 36 (2) (2018) 02C108.

25. **Gabdullin P., Zhurkin A., Osipov V., et al.,** Thin carbon films: Correlation between morphology and field-emission capability, Diam. Relat. Mater. 105 (May) (2020) 107805.

26. **Eidelman E. D., Arkhipov A. V.,** Field emission from carbon nanostructures: Models and experiment, Phys.–Usp. 63 (7) (2020) 648–667.

27. **Bogachek E. N., Kulik I. O., Omel'yanchuk A. N., Shkorbatov A. G.,** Drag-related thermo-emf in metallic systems containing a point contact, JETP Lett. 41 (12) (1985) 633–636.

28. **Shklyarevskii O. I., Jansen A. G. M., Hermsen J. G. H., Wyder P.,** Thermoelectric voltage between identical metals in a point-contact configuration, Phys. Rev. Lett. 57 (11) (1986) 1374–1377.

29. **Trzcinski R., Gmelin E., Queisser H. J.,** Quenched phonon drag in silicon microcontacts, Phys. Rev. Lett. 56 (10) (1986) 1086–1089.

30. **Weber L., Lehr M., Gmelin E.,** Reduction of the thermopower in semiconducting point contacts, Phys. Rev. B. 46 (15) (1992) 9511–9514.

31. **Mahan G. D., Claro F.,** Nonlocal theory of thermal conductivity, Phys. Rev. B. 38 (3) (1988) 1963–1969.

32. **Mahan G. D.,** The Benedicks effect: Nonlocal electron transport in metals, Phys. Rev. B. 43 (5) (1991) 3945–3951.

33. **Grigorenko A. N., Nikitin P. I., Jelski D. A., George T. F.,** Thermoelectric phenomena in metals under large temperature gradients, J. Appl. Phys. 69 (5) (1991) 3375–3377.

34. **Vermeersch B., Shakouri A.,** Nonlocality in microscale heat conduction, https://api.semanticscholar.org/CorpusID:118469205. (Accessed September 11, 2023).

35. **Koh Y. K., Cahill D. G., Sun B.,** Nonlocal theory for heat transport at high frequencies, Phys. Rev. B. 90 (20) (2014) 205412.

36. **Ezzahri Y., Joulain K., Ordonez-Miranda J.,** Heat transport in semiconductor crystals: Beyond the local-linear approximation, J. Appl. Phys. 128 (10) (2020) 105104.

37. **Baratifarimani R., Shomali Z.,** Implementation of nonlocal non-Fourier heat transfer for semiconductor nanostructures, https://api.semanticscholar.org/CorpusID:259317109 (Accessed September 11, 2023).

38. **Cahill D. G., Ford W. K., Goodson K. E., et al.,** Nanoscale thermal transport, J. Appl. Phys. 93 (2) (2003) 793–818.

39. **Wang C., Chen F., Sun K., et al.,** Instruments for measuring Seebeck coefficient of thin film thermoelectric materials: A mini-review, Rev. Sci. Instrum. 89 (10) (2018) 101501.

40. **Kim S. J., We J. H., Kim G. S., Cho B. J.,** Simultaneous measurement of the Seebeck coefficient and thermal conductivity in the cross-sectional direction of thermoelectric thick film, J. Appl. Phys. 112 (10) (2012) 104511.

41. **Majumdar A.,** Scanning thermal microscopy, Annu. Rev. Mater. Sci. 29 (1) (1999) 505–585.

42. **Shi L., Plyasunov S., Bachtold A., et al.,** Scanning thermal microscopy of carbon nanotubes using batch-fabricated probes, Appl. Phys. Lett. 77 (26) (2000) 4295–4297.

43. **Fletcher P. C., Lee B., King W. P.,** Thermoelectric voltage at a nanometer-scale heated tip point contact, Nanotechnology. 23 (3) (2011) 035401.

44. **Nakamoto G., Nakabayashi Y.,** Development of a two dimensional scanning Seebeck coefficient measurement system by a micro-probe method, Intermetallics. 32 (Jan) (2013) 233–238.

45. **Tan A., Sadat S., Reddy P.,** Measurement of thermopower and current-voltage characteristics of molecular junctions to identify orbital alignment, Appl. Phys. Lett. 96 (1) (2010) 013110.

46. **Cahill D. G., Braun P. V., Chen G., et al.,** Nanoscale thermal transport. II. 2003–2012, Appl. Phys. Rev. 1 (1) (2014) 011305.

47. **De Boor J., Müller E.,** Data analysis for Seebeck coefficient measurements, Rev. Sci. Instrum. 84 (6) (2013) 065102.

48. **Bizyaev I., Gabdullin P., Chumak M., et al.,** Low-field electron emission capability of thin films on flat silicon substrates: Experiments with Mo and general model for refractory metals and carbon, Nanomaterials. 11 (12) (2021) 3350.

49. **Arkhipov A. V., Eidelman E. D., Zhurkin A. M., et al.,** Low-field electron emission from carbon cluster films: Combined thermoelectric/hot-electron model of the phenomenon, Fuller. Nanotub. Car. N. 28 (4) (2020) 286–294.

50. **Weber L., Gmelin E.,** A new device for transport measurements on point contacts, Rev. Sci. Instrum. 63 (1) (1992) 211–217.

51. **Williams C. C., Wickramasinghe H. K.,** Scanning thermal profiler, Appl. Phys. Lett. 49 (23) (1986) 1587–1589.

СПИСОК ЛИТЕРАТУРЫ

1. **Sadeghi H.** Quantum and phonon interference-enhanced molecular-scale thermoelectricity // The Journal of Physical Chemistry C. 2019. Vol. 123. No. 20. Pp. 12556–12562.

2. **Karlstrцm O., Linke H., Karlstrцm G., Wacker A.** Increasing thermoelectric performance using coherent transport // Physical Review B. 2011. Vol. 84. No. 11. P. 113415.

3. **Mahan G. D., Sofo J. O.** The best thermoelectric // Proceedings of the National Academy of Sciences of the USA. 1996. Vol. 93. No. 15. Pp. 7436–7439.

4. **Дмитриев А. С.** Введение в нанотеплофизику. 2-е изд., электронное. М.: Лаборатория знаний, 2020. 793 с.

5. **Zevalkink A., Smiadak D. M., Blackburn J. L., et al.** A practical field guide to thermoelectrics: Fundamentals, synthesis, and characterization // Applied Physics Reviews. 2018. Vol. 5. No. 2. P. 021303.

6. **Lyeo H. K., Khajetoorians A. A., Shi L., Pipe K. P., Ram R. J., Shakouri A., Shih C. K.** Profiling the thermoelectric power of semiconductor junctions with nanometer resolution // Science. 2004. Vol. 303. No. 5659. Pp. 816–818.

7. **Ikeda H., Salleh F.** Influence of heavy doping on Seebeck coefficient in silicon-on-insulator // Applied Physics Letters. 2010. Vol. 96. No. 1. P. 012106.

8. **Salleh F., Suzuki Y., Miwa K., Ikeda H.** Modulation of Seebeck coefficient for silicon-on-insulator layer induced by bias-injected carriers // Applied Physics Letters. 2013. Vol. 103. No. 6. P. 062107.

9. **Tretiakov O. A., Abanov Ar., Sinova J.** Holey topological thermoelectrics // Applied Physics Letters. 2011. Vol. 99. No. 11. P. 113110.

10. **Krali E., Durrani Z. A. K.** Seebeck coefficient in silicon nanowire arrays // Applied Physics Letters. 2013. Vol. 102. No. 14. P. 143102.

11. **Taniguchi T., Terada T., Komatsubara Y., Ishibe T., Konoike K., Sanada A., Naruse N., Mera Y., Nakamura Y.** Phonon transport in the nano-system of Si and SiGe films with Ge nanodots and approach to ultralow thermal conductivity // Nanoscale. 2021. Vol. 13. No. 9. Pp. 4971–4977.

12. **Bergfield J. P., Solis M. A., Stafford C. A.** Giant thermoelectric effect from transmission supernodes // ACS (American Chemical Society) Nano. 2010. Vol. 4. No. 9. Pp. 5314–5320.

13. **Хвесюк В. И., Скрябин А. С.** Теплопроводность наноструктур // Теплофизика высоких температур. 2017. Т. 55. № 3. С. 447–471.

14. **Dubi Y., Di Ventra M.** Colloquium: Heat flow and thermoelectricity in atomic and molecular junctions // Reviews of Modern Physics. 2011. Vol. 83. No. 1. Pp. 131–155.

15. **Sadeghi H., Sangtarash S., Lambert C. J**. Oligoyne molecular junctions for efficient room temperature thermoelectric power generation // Nano Letters. 2015. Vol. 15. No. 11. Pp. 7467–7472.

16. **Cui L., Miao R., Wang K., Thompson D., Zotti L. A., Cuevas J. C., Meyhofer E., Reddy P.** Peltier cooling in molecular junctions // Nature Nanotechnology. 2018. Vol. 13. No. 2. Pp. 122–127.

17. **Liu C., Lu P., Chen W., Zhao Y., Chen Y.** Phonon transport in graphene based materials // Physical Chemistry, Chemical Physics. 2021. Vol. 23. No. 46. Pp. 26030–26060.

18. **Варламов А. А., Кавокин А. В., Лукьянчук И. А., Шарапов С. Г.** Аномальные термоэлектрические и термомагнитные свойства графена // Успехи физических наук. 2012. Т. 182. № 11. С. 1229–1234.

19. **Wu Q., Sadeghi H., Garcна-Suбrez V. M., Ferrer J., Lambert C. J.** Thermoelectricity in vertical graphene-C_{60}-graphene architectures // Scientific Reports. 2017. Vol. 7. 15 September. P. 11680.

20. **Эйдельман Е. Д.** Термоэлектрический преобразователь с рекордными параметрами на основе углеродных наноструктур: разработка научных основ // Физика и техника полупроводников. 2017. Т. 51. № 7. С. 944–947.

21. **Эйдельман Е. Д.** Термоэлектрический эффект и термоэлектрический генератор на основе углеродных наноструктур: достижения и перспективы // Успехи физических наук. 2021. Т. 191. № 6. С. 561–585.

22. **Eydelman E. D., Vul' A. Ya.** The strong thermoelectric effect in nanocarbon generated by ballistic phonon drag of electrons // Journal of Physics: Condensed Matter. 2007. Vol. 19. No. 7. Pp. 266210–266223.

23. **Koniakhin S.V., Eidelman E. D.** Phonon drag thermopower in graphene in equipartition regime // Europhysics Letters. 2013. Vol. 103. No. 3. P. 37006.

24. **Andronov A., Budylina E., Shkitun P., Gabdullin P., Gnuchev N., Kvashenkina O., Arkhipov A.**

Characterization of thin carbon films capable of low-field electron emission // Journal of Vacuum Science & Technology B. 2018. Vol. 36. No. 2. P. 02C108.

25. **Gabdullin P., Zhurkin A., Osipov V., Besedina N., Kvashenkina O., Arkhipov A.** Thin carbon films: Correlation between morphology and field-emission capability // Diamond & Related Materials. 2020. Vol. 105. May. P. 107805.

26. **Эйдельман Е. Д., Архипов А. В.** Полевая эмиссия из углеродных наноструктур: модели и эксперимент // Успехи физических наук. 2020. Т. 190. № 7. С. 693–714.

27. **Богачек Э. Н., Кулик И. О., Омельянчук А. Л., Шкорбатов А. Г.** Термоэдс увлечения в металлических системах, содержащих микроконтакт // Письма в Журнал экспериментальной и теоретической физики. 1985. Т. 41. № 12. С. 519–521.

28. **Shklyarevskii O. I., Jansen A. G. M., Hermsen J. G. H., Wyder P.** Thermoelectric voltage between identical metals in a point-contact configuration // Physical Review Letters. 1986. Vol. 57. No. 11. Pp. 1374–1377.

29. **Trzcinski R., Gmelin E., Queisser H. J.** Quenched phonon drag in silicon microcontacts // Physical Review Letters. 1986. Vol. 56. No. 10. Pp. 1086–1089.

30. **Weber L., Lehr M., Gmelin E.** Reduction of the thermopower in semiconducting point contacts // Physical Review B. 1992. Vol. 46. No. 15. 9511–9514.

31. **Mahan G. D., Claro F.** Nonlocal theory of thermal conductivity // Physical Review B. 1988. Vol. 38. No. 3. Pp. 1963–1969.

32. **Mahan G. D.** The Benedicks effect: Nonlocal electron transport in metals // Physical Review B. 1991. Vol. 43. No. 5. Pp. 3945–3951.

33. **Grigorenko A. N., Nikitin P. I., Jelski D. A., George T. F.** Thermoelectric phenomena in metals under large temperature gradients // Journal of Applied Physics. 1991. Vol. 69. No. 5. Pp. 3375–3377.

34. **Vermeersch B., Shakouri A.** Nonlocality in microscale heat conduction. https://api.semanticscholar.org/CorpusID:118469205 (Дата обращения 11.09.2023).

35. **Koh Y. K., Cahill D. G., Sun B.** Nonlocal theory for heat transport at high frequencies // Physical Review B. 2014. Vol. 90. No. 20. P. 205412.

36. **Ezzahri Y., Joulain K., Ordonez-Miranda J.** Heat transport in semiconductor crystals: Beyond the local-linear approximation // Journal of Applied Physics. 2020. Vol. 128. No. 10. P. 105104.

37. **Baratifarimani R., Shomali Z.** Implementation of nonlocal non-Fourier heat transfer for semiconductor nanostructures. https://api.semanticscholar.org/ CorpusID:259317109 (Дата обращения 11.09.2023).

38. **Cahill D. G., Ford W. K., Goodson K. E., Mahan G. D., Majumdar A., Maris H. J., Merlin R., Phillpot S. R.** Nanoscale thermal transport // Journal of Applied Physics. 2003. Vol. 93. No. 2. Pp. 793–818.

39. **Wang C., Chen F., Sun K., Chen R., Li M., Zhou X., Sun Y., Chen D., Wang G.** Instruments for measuring Seebeck coefficient of thin film thermoelectric materials: A mini-review // Review of Scientific Instruments. 2018. Vol. 89. No. 10. P. 101501.

40. **Kim S. J., We J. H., Kim G. S., Cho B. J.** Simultaneous measurement of the Seebeck coefficient and thermal conductivity in the cross-sectional direction of thermoelectric thick film // Journal of Applied Physics. 2012. Vol. 112. No. 10. P. 104511.

41. **Majumdar A.** Scanning thermal microscopy // Annual Review of Materials Science. 1999. Vol. 29. No. 1. Pp. 505–585.

42. **Shi L., Plyasunov S., Bachtold A., McEuen P. L., Majumdar A.** Scanning thermal microscopy of carbon nanotubes using batch-fabricated probes // Applied Physics Letters. 2000. Vol. 77. No. 26. Pp. 4295–4297.

43. **Fletcher P. C., Lee B., King W. P.** Thermoelectric voltage at a nanometer-scale heated tip point contact // Nanotechnology. Vol. 23. No. 3. P. 035401.

44. **Nakamoto G., Nakabayashi Y.** Development of a two dimensional scanning Seebeck coefficient measurement system by a micro-probe method // Intermetallics. 2013. Vol. 32. January. Pp. 233–238.

45. **Tan A., Sadat S., Reddy P.** Measurement of thermopower and current-voltage characteristics of molecular junctions to identify orbital alignment // Applied Physics Letters. 2010. Vol. 96. No. 1. P. 013110.

46. **Cahill D. G., Braun P. V., Chen G., et al.** Nanoscale thermal transport. II. 2003–2012 // Applied Physics Reviews. 2014. Vol. 1. No. 1. P. 011305.

47. **De Boor J., Müller E.** Data analysis for Seebeck coefficient measurements // Review of Scientific Instruments. 2013. Vol. 84. No. 6. P. 065102.

48. **Bizyaev I., Gabdullin P., Chumak M., Babyuk V., Davydov S., Osipov V., Kuznetsov A., Kvashenkina O., Arkhipov A.** Low-field electron emission capability of thin films on flat silicon substrates: Experiments with Mo and general model for refractory metals and carbon // Nanomaterials. 2021. Vol. 11. No. 12. P. 3350.

49. **Arkhipov A. V., Eidelman E. D., Zhurkin A. M., Osipov V. S., Gabdullin P. G.** Low-field electron emission from carbon cluster films: Combined thermoelectric/hot-electron model of the phenomenon // Fullerenes, Nanotubes and Carbon Nanostructures. 2020. Vol. 28. No. 4. Pp. 286–294.

50. **Weber L., Gmelin E.** A new device for transport measurements on point contacts // Review of Scientific Instruments. 1992. Vol. 63. No. 1. Pp. 211–217.

51. **Williams C. C., Wickramasinghe H. K.** Scanning thermal profiler // Applied Physics Letters. 1986. Vol. 49. No. 23. Pp. 1587–1589.

THE AUTHORS

TROFIMOVICH Karina R.
Peter the Great St. Petersburg Polytechnic University
29 Politechnicheskaya St., St. Petersburg, 195251, Russia
karina-khasanova-2001@mail.ru

GABDULLIN Pavel G.
Peter the Great St. Petersburg Polytechnic University
29 Politechnicheskaya St., St. Petersburg, 195251, Russia
gabdullin_pg@spbstu.ru
ORCID: 0000-0002-2519-2577

ARKHIPOV Alexander V.
Peter the Great St. Petersburg Polytechnic University
29 Politechnicheskaya St., St. Petersburg, 195251, Russia
arkhipov@rphf.spbstu.ru
ORCID: 0000-0002-3321-7797

СВЕДЕНИЯ ОБ АВТОРАХ

ТРОФИМОВИЧ Карина Робертовна – *студентка Института электроники и телекоммуникаций Санкт-Петербургского политехнического университета Петра Великого, Санкт-Петербург, Россия.*
195251, Россия, г. Санкт-Петербург, Политехническая ул., 29
karina-khasanova-2001@mail.ru

ГАБДУЛЛИН Павел Гарифович – *кандидат технических наук, доцент, директор Научно-технологического центра «Нейропрогнозирование материалов и технологий электронной промышленности» Санкт-Петербургского политехнического университета Петра Великого, Санкт-Петербург, Россия.*
195251, Россия, г. Санкт-Петербург, Политехническая ул., 29
gabdullin_pg@spbstu.ru
ORCID: 0000-0002-2519-2577

АРХИПОВ Александр Викторович – *доктор физико-математических наук, профессор Высшей инженерно-физической школы Санкт-Петербургского политехнического университета Петра Великого, Санкт-Петербург, Россия.*

195251, Россия, г. Санкт-Петербург, Политехническая ул., 29

arkhipov@rphf.spbstu.ru

ORCID: 0000-0002-3321-7797

Received 16.09.2023. Approved after reviewing 01.12.2023. Accepted 01.12.2023.

Статья поступила в редакцию 16.09.2023. Одобрена после рецензирования 01.12.2023. Принята 01.12.2023.